

# Folding and insertion thermodynamics of the transmembrane WALP peptide

Tristan Berau,<sup>1, a)</sup> W. F. Drew Bennett,<sup>2</sup> Jim Pfaendtner,<sup>3</sup> Markus Deserno,<sup>4</sup> and Mikko Karttunen<sup>5</sup>

<sup>1)</sup>Max Planck Institute for Polymer Research, Ackermannweg 10, 55128 Mainz, Germany

<sup>2)</sup>Department of Chemistry, University of Waterloo, 200 University Avenue West, Waterloo, Ontario, Canada N2L 3G1

<sup>3)</sup>Department of Chemical Engineering, University of Washington, Seattle, Washington, United States

<sup>4)</sup>Department of Physics, Carnegie Mellon University, Pittsburgh, PA 15213, United States

<sup>5)</sup>Department of Mathematics and Computer Science & Institute for Complex Molecular Systems, Eindhoven University of Technology - P.O. Box 513, MetaForum, 5600 MB, Eindhoven, The Netherlands

(Dated: 31 August 2015)

The anchor of most integral membrane proteins consists of one or several helices spanning the lipid bilayer. The WALP peptide,  $\text{GWW(LA)}_n\text{(L)WWA}$ , is a common model helix to study the fundamentals of protein insertion and folding, as well as helix-helix association in the membrane. Its structural properties have been illuminated in a large number of experimental and simulation studies. In this combined coarse-grained and atomistic simulation study, we probe the thermodynamics of a single WALP peptide, focusing on both the insertion across the water-membrane interface, as well as folding in both water and a membrane. The potential of mean force characterizing the peptide's insertion into the membrane shows qualitatively similar behavior across peptides and three force fields. However, the Martini force field exhibits a pronounced secondary minimum for an adsorbed interfacial state, which may even become the global minimum—in contrast to both atomistic simulations and the alternative PLUM force field. Even though the two coarse-grained models reproduce the free energy of insertion of individual amino acids side chains, they both underestimate its corresponding value for the full peptide (as compared with atomistic simulations), hinting at cooperative physics beyond the residue level. Folding of WALP in the two environments indicates the helix as the most stable structure, though with different relative stabilities and chain-length dependence.

## I. INTRODUCTION

Transmembrane proteins constitute one of the most important biological building blocks, enabling communication of material and information between a cell and its environment, or between different intracellular compartments.<sup>1–4</sup> Despite impressive progress in determining membrane protein structures,<sup>5</sup> aided by technological advances in fields such as electron tomography<sup>6</sup> and femtosecond crystallography,<sup>7</sup> the number of known structures still lags far behind the case of soluble proteins. Unfortunately, in the absence of structures, the options for numerical modeling are limited. This is true not only because protein structure prediction remains a formidable computational challenge, both for equilibration and force-field reasons.<sup>8–11</sup> We also face the additional predicament that a lipid bilayer and its surroundings constitute a very highly anisotropic environment, where everything from dielectric constants to lateral stresses varies dramatically on an Ångström scale, pushing both continuum theory and local thermodynamics to their limits. It should hence not come as a surprise that even ostensibly basic questions about structure, location and interaction of small peptides in bilayers remain difficult to answer.<sup>12</sup>

The overwhelming majority of integral membrane proteins is anchored into the lipid bilayer by one or several transmembrane  $\alpha$ -helices, followed to a much smaller fraction by proteins where a  $\beta$ -barrel motif takes over that role.<sup>13,14</sup> This is rationalized by the hydrophobic environment of the lipid tails, which favors protein conformations that minimize the number of broken backbone hydrogen bonds.<sup>15,16</sup>

In an effort to better understand membrane proteins at a biophysical level, a large body of work has focused on studying individual model helices. One common example is the sequence of WALP peptides, composed of alternating alanine and leucine residues and flanked by two tryptophans at each terminus. It was designed to resemble a transmembrane helix in membrane proteins, while permitting an easy way to change its length.<sup>17,18</sup> The arrangement of residues is such that WALP16 corresponds to the sequence  $\text{GWW(LA)}_5\text{WWA}$ , while longer WALP peptides include more LA repeat units (and occasionally an additional alanine between the final leucine and the C-terminal tryptophans).

Various experimental and simulation studies have shed light on the stability of WALP as a transmembrane helix. Experimentally, a combination of NMR methods, hydrogen/deuterium exchange, and mass spectrometry applied to WALP of different chain lengths, as well as lipids of different size, have provided important insight into the role of hydrophobic mismatch—the difference

<sup>a)</sup>Electronic mail: berau@mpip-mainz.mpg.de

between the length of a peptide’s hydrophobic stretch and that of the bilayer’s hydrophobic core.<sup>17,18</sup> For instance, a positive mismatch leads to an average tilt angle between the peptide and the membrane normal, a quantity that can be determined from both experiments (e.g., quadrupolar splittings from  $^2\text{H}$  solid-state NMR<sup>19</sup>) and computer simulations.<sup>20–22</sup> Notably, Monticelli *et al.* resolved an apparent discrepancy between the average tilt angle extracted from experiment versus the same observable calculated in molecular dynamics simulations. Using a coarse-grained model, and hence being able to access much longer time scales, they showed that both experiment and simulation agree, thus highlighting the importance of sampling the tilt angle over the microsecond time scales relevant for NMR experiments.<sup>23</sup> Atomistic simulations later confirmed these findings using enhanced-sampling methodologies.<sup>24</sup>

These studies illuminate the thermodynamics of transmembrane helices—not only the stability in the membrane, but also the insertion from water. Using an atomistic representation for peptides, but an *implicit* water/membrane model, Im and Brooks showed that WALP{16,19,23}, starting as an initial random coil, would spontaneously insert and fold into a bilayer.<sup>20</sup> Further, Nymeyer *et al.*<sup>25</sup> and Ulmschneider *et al.*<sup>26</sup> demonstrated insertion and folding of WALP16 in an *explicit* DPPC membrane using enhanced-sampling methodologies and high-temperature simulations, respectively, to alleviate the considerable sampling issues. Some of us reported similar findings using PLUM, a recently-developed CG model,<sup>27</sup> with and without enhanced sampling.<sup>28</sup>

The potential of mean force (PMF) for the insertion of WALP across a water/membrane interface provides insight into the thermodynamics of insertion: both in terms of the free-energy difference between the two environments and the possible existence of intermediate barriers. Structurally, WALP is known to form a helix in the membrane, but its conformation in water is largely unknown, because its many hydrophobic residues render it prone to aggregation at experimentally relevant concentrations. Insertion simulations, on the other hand, typically work with a single peptide (due to sampling limitations). However, their ability to predict WALP structures in solution is not merely a matter of the required computational resources, but also of the model’s ability to *describe* secondary structure changes in the first place. For instance, Bond *et al.* used CG simulations to study the thermodynamics of insertion of WALP into a DPPC bilayer. Their model, a variant of the CG Martini force field,<sup>29</sup> required them to constrain the peptide into a helix in all environments,<sup>30</sup> which begs the question whether a potential folding/unfolding equilibrium contributes to the free energy of insertion. One aim of our present study is to address this question.

The following work investigates the link between WALP’s structure and its environment. We rely on the CG PLUM force field<sup>27</sup> to efficiently sample the thermo-

dynamics of insertion across the water-membrane interface, without explicit bias on the secondary structure. To gauge the robustness of the results, we carry out equivalent simulations using both the CG Martini force field<sup>29</sup>, bearing in mind its secondary-structure constraints, as well as atomistic simulations, despite unavoidable challenges associated with sampling. While the results agree in many qualitative features, we find a number of interesting exceptions which we analyze in some detail. In addition, the free-energy profile as a function of helicity in both the membrane and water environments provide insight into the preferred conformations.

## II. SIMULATION MODELS

### A. Coarse-grained simulations: PLUM force field

The following describes the CG PLUM force field. The associated simulation protocol and parameters used in this work are described in Appendix A.

The PLUM force field is constructed from the cross-parametrization of implicit-solvent CG peptide<sup>31</sup> and lipid<sup>32,33</sup> models, which we summarize in the following.

The peptide model includes amino-acid specificity and can stabilize different secondary structures using a single parametrization, i.e., without explicit bias toward one particular conformation. Each amino acid is described using four beads: one for the side chain and three for the backbone, providing enough resolution to describe backbone dihedrals. Phenomenological interactions allow the model to reproduce basic properties of peptides and proteins, such as excluded volume, hydrophobicity, and hydrogen bonds. The model was tuned to qualitatively reproduce the Ramachandran plot of tripeptides and fold a *de novo* three-helix bundle. Without changing the force-field parameters, the model can also stabilize different helical peptides and assemble  $\beta$ -sheet-rich oligomers.<sup>31</sup> The CG model has been applied to a variety of scenarios involving helical peptides,<sup>34,35</sup> aggregation of  $\beta$ -rich peptides,<sup>36</sup> and  $\beta$ -barrel formation at the interface between virus capsid proteins.<sup>37</sup>

The lipid model maps a 1-palmitoyl-2-oleoyl-sn-glycero-3-phosphocholine (POPC) lipid into 16 beads, using 8 bead types to distinguish different chemical moieties.<sup>32</sup> Interaction potentials were determined from an iterative-Boltzmann inversion<sup>38</sup> of the radial distribution functions, obtained from an all-atom POPC membrane simulation. Being an implicit solvent model, the absence of water is compensated by a phenomenological attractive interaction between tail beads. Free lipids self-assemble into a bilayer, which then reproduces elastic properties (e.g., the bending modulus), the mass density profile, and the orientation of intramolecular bonds.<sup>32</sup> Other neutral lipids can be constructed from the set of bead types and reach satisfying transferability in terms of structure, area per lipid, and temperature dependence of the main phase transition.<sup>33</sup>

While keeping the individual force-field parameters fixed, the cross-parameters between the peptide and lipid beads were optimized to reproduce atomistic potential of mean force (PMF) curves of the insertion of single amino-acid side chains into a DOPC bilayer.<sup>39</sup> The cross-parametrization was validated by investigating a number of structural properties specific to membrane peptides, such as tilt angle, hydrophobic mismatch, and transient pore formation from the cooperative action of antimicrobial peptides.<sup>27</sup> More recently, the use of a Hamiltonian replica exchange algorithm (more below) assisted in folding several peptides inside the membrane: WALP{16,19,23}, as well as the 50-residue-long major pVIII coat protein (fd coat) of the filamentous fd bacteriophage.<sup>28</sup>

### B. Coarse-grained simulations: Martini force field

Though Martini is a commonly used force field for the description of peptide-lipid interactions, we highlight some of the key differences with PLUM for completeness. The simulation details used throughout this work can be found in Appendix B.

The coarse-grained Martini model maps on average four non-hydrogen atoms into one CG bead, and it can describe a wide variety of biomolecules, e.g., water, lipids, proteins, carbohydrates, or small molecules.<sup>29,40–43</sup> The key idea is to represent characteristic chemical moieties with a limited set of CG bead types, determined from the overall charge, hydrogen-bond capability, and water/oil partitioning coefficient.<sup>29</sup>

Martini reproduces a number of lipid-membrane characteristics: self-assembly, area per lipid, elastic properties, as well as a reasonable bilayer stress profile.<sup>29</sup> A particularly attractive feature of the model is that its building-block approach eases the construction of a large variety of molecules, in particular many lipids<sup>44</sup> and sterols.<sup>29</sup> Due to the mapping of 3 – 4 heavy atoms to 1 bead there can be some ambiguity with regards to the optimal mapping of molecular fragments. For POPC, the oleyl tail was originally modeled with 5 beads,<sup>29</sup> while an updated model uses 4 beads.<sup>45</sup>

Martini has been extended to proteins, focusing mainly on peptide-bilayer interactions.<sup>40,41</sup> The parametrization quite accurately captures the free-energy of the insertion of single amino acid side chains and reproduces a number of structural properties of model transmembrane helices. Though Martini tends to map a similar number of beads per amino acid as PLUM, the emphasis is different: a single bead represents the backbone while several beads constitute each side chain, providing a better description of the sterics. The single-backbone bead description necessitates the use of secondary-structure restraints, present in the form of torsional parameters specific to different folds (e.g.,  $\alpha$ -helix or  $\beta$ -sheet). As a result, peptides modeled with Martini cannot (un)fold or refold during the simulation.

### C. Atomistic simulations

The simulation protocol of the atomistic simulations is detailed in Appendix C.

## III. RESULTS

### A. Insertion thermodynamics

Fig. 1 compares the thermodynamics of insertion of a single WALP{16,19,23} peptide into a POPC membrane using different force fields. In each case, the potential of mean force (PMF) is displayed as a function of the distance  $z$  between the peptide’s center of mass and that of the membrane, which we take as a proxy for its midplane. We extended calculations up to  $z = 5$  nm to ensure that the peptide was entirely out of the membrane.

In previous studies, which investigated the insertion of single amino acids,<sup>27,39</sup> the bilayer nature was exploited by simultaneously inserting amino acids into both leaflets. This not only increased statistics but also minimized conceivable artifacts due to bilayer asymmetry. In our case the size of a peptide makes this strategy unfeasible, raising the question how the PMF is affected by this asymmetric insertion, which stresses the two leaflets differently. In Appendix E we calculate the resulting elastic correction and show it to be negligible.

Fig.1 (a) shows the PMF of WALP16, WALP19, and WALP23 using the PLUM force field. All curves indicate that the peptide prefers the bilayer over the water environment—an expected feature given the hydrophobicity of the amino acids, and in line with the results of Bond *et al.*<sup>30</sup> As we increase the peptide’s length, and hence the number of hydrophobic amino acids, the free energy of the fully inserted state becomes successively smaller. At the bilayer midplane ( $z = 0$ ), each residue contributes on average 1.5 kcal/mol to the free energy of insertion. For each PMF, we identify three plateaus: (i) close to the bilayer midplane ( $z \approx 0$ ) the protein samples transmembrane conformations; (ii) around the bilayer’s interfacial region ( $z \approx 2$  nm) the peptide is still helical, but oriented *parallel* to the surface of the membrane; and finally (iii) the asymptotic region ( $z \gtrsim 4$  nm) where the peptide has left the membrane and so its free energy no longer depends on  $z$ . Representative conformations are shown in Fig. 2 for WALP16, illustrating the transition from fully transmembrane to interfacial to desorbed. Notice in particular the significant membrane deformation occurring at  $z \approx 3$  nm (see Fig. 2 (d)). It occurs because the peptide’s free energy gain for staying in contact with the membrane outweighs the cost of the concomitant elastic deformation—at least for some range of  $z$ -values. Kopelevich recently showed that these deformations lead to an underestimation of the free-energy barrier upon insertion, though the overall free-energy difference should be accurate.<sup>46</sup>

Compared to the PLUM results, the PMFs computed

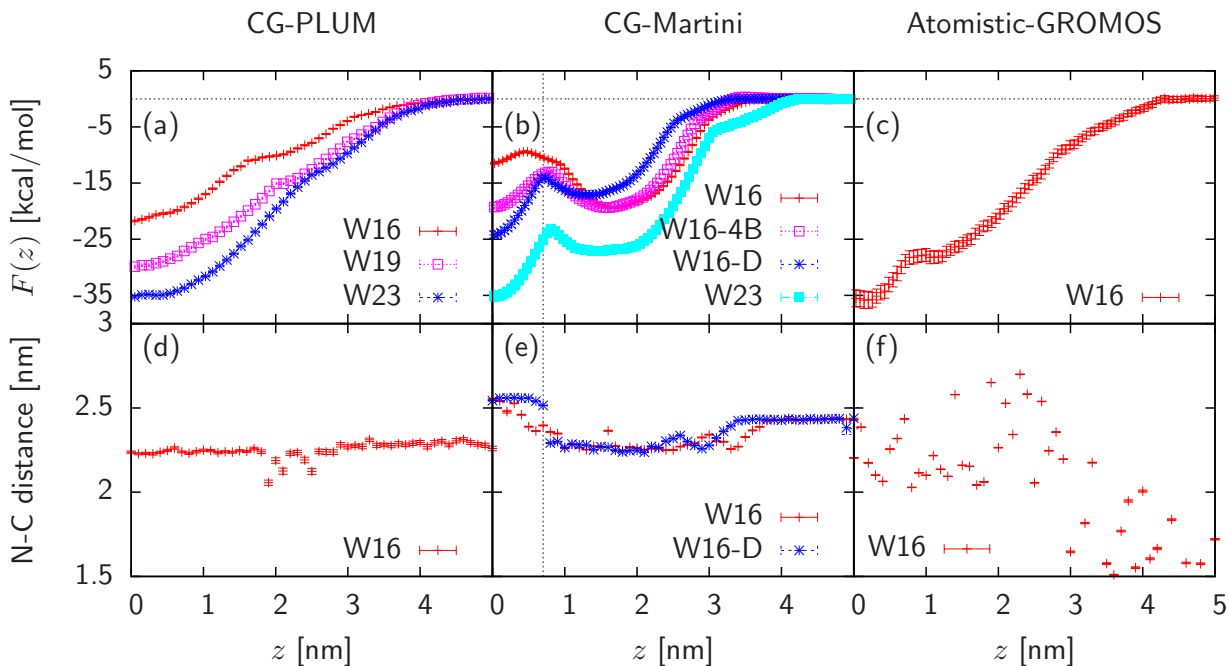


FIG. 1. Potential of mean force curves as a function of the distance from the bilayer midplane,  $z$ : (a) WALP{16,19,23} from the PLUM force field; (b) WALP16 in POPC (“W16”), WALP16 in POPC using the updated force field<sup>45</sup> with four beads for the oleoyl chain (“W16-4B”), WALP16 in DMPC (“W16-D”), and WALP23 in POPC (“W23”) using the Martini model with standard water. Note that W16 using Martini’s polarizable water yielded virtually identical results (data not shown); (c) WALP16 using the all-atom GROMOS force field. The PLUM energies are mapped from the reduced unit  $\mathcal{E} = 0.617$  kcal/mol. (d), (e), and (f): N-C terminus distance (measured from  $C_\alpha$  to  $C_\alpha$ ) for the respective models. The error of the mean is displayed. Note the larger N-C distance for Martini in DMPC (e) close to the bilayer midplane.

with the Martini model (Fig. 1 (b)) have a noticeably different shape. Specifically, all curves exhibit a secondary minimum corresponding to the interfacial state, irrespective of whether the standard or the polarizable water model is used (the two curves overlap, only one of them is shown). While this interfacial state also exists for the PLUM model, as Fig. 2 (c) indicates, its impact on the PMF appears much stronger in the Martini model. In fact, for WALP16 in a POPC membrane the interfacial state is even lower in free energy than the completely inserted transmembrane state, and hence Martini makes a qualitatively different prediction from PLUM about thermal equilibrium. In agreement with these results, a spontaneous transition from transmembrane to interfacial states was previously observed by Ramadurai *et al.*<sup>48</sup> using unrestrained simulations of WALP16 in lipid membranes made of five or six tailbead-long Martini lipids—analogueous to the current POPC parametrization. In fact, these authors only saw transmembrane-WALP16 spontaneously transition into the interfacial state when they used lipids with long chains. While they did not measure a PMF, the barrier from transmembrane to interfacial (Fig. 1 (b);  $\approx 2$  kcal/mol) calculated by us indeed suggests the possibility to observe such an event spontaneously, given reasonably long simulations.

To test whether this behavior originates from the

negative hydrophobic mismatch between WALP16 and POPC, we conducted two control simulations: first, we kept WALP16 but inserted it into a thinner DMPC bilayer; and second, we kept the POPC bilayer but used the longer WALP23 peptide. The resulting PMFs (Fig. 1 (b)) show that in both cases the transmembrane state becomes the most favorable one, even though the interfacial state continues to produce a very noticeable metastable minimum. This mirrors the observation of Bond *et al.*, who studied WALP23 in DPPC using a customized version of the Martini model.<sup>30</sup>

We measured the membrane thickness from the distribution of distances between the phosphate groups and the bilayer midplane projected along the membrane normal. While PLUM and GROMOS yield similar distributions that peak around 1.8 nm, Martini stabilizes a thicker membrane with a peak around 2.1 nm (Fig. 3). To compare the impact on the alignment of the peptide, we probed the distribution of distances between the tryptophan side chains and the bilayer midplane, similarly projected along the membrane normal. Here again, PLUM and GROMOS yield distributions that peak around the same point, though the atomistic distribution broadens at lower distances. Martini, on the other hand, samples a distribution shifted by  $\approx 0.1$  nm to higher values. The differences in offsets between the tryptophan and

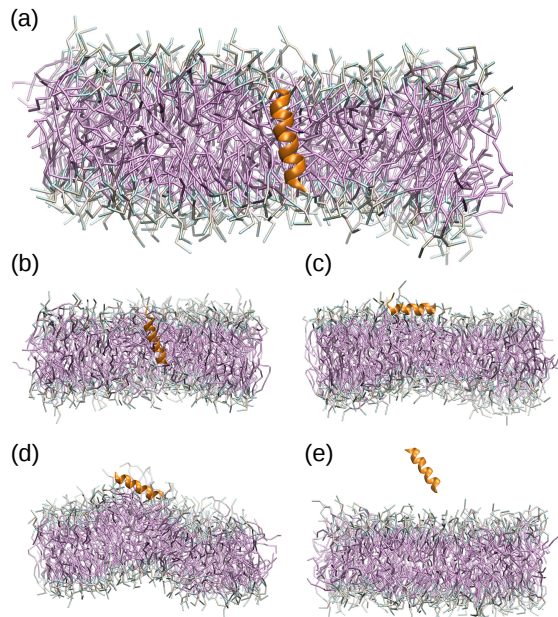


FIG. 2. Representative conformations of the WALP16 insertion in POPC using the PLUM force field at different distances from the bilayer midplane,  $z$ : (a)  $z = 0$ , (b)  $z = 1$  nm, (c)  $z = 2$  nm, (d)  $z = 3$  nm, and (e)  $z = 4$  nm. The peptide is depicted in orange, where thick and thin ribbons correspond to the helical and coil states, respectively; the lipids are color-coded according to their bead type: purple for the hydrocarbon chains, light pastel colors for the interfacial and head groups. Rendered with VMD.<sup>47</sup>

phosphate distributions indicate that Martini’s thicker membrane will result in the tryptophan side chains being buried deeper inside the membrane. Such a deeper insertion will result in a larger energetic penalty, as evidenced by the PMF curves of individual side chains<sup>27,39,40</sup> (sampled using the OPLS force field,<sup>49</sup> not GROMOS).

While the current investigation relied on the original POPC Martini model made of five beads for the oleoyl chain, Wassenaar *et al.* recently introduced a parametrization using only four beads, thereby reducing slightly the membrane thickness.<sup>45</sup> The PMF corresponding to the updated force field is shown in Fig. 1 (b), “W16-4B”. The reduced hydrophobic mismatch between the thinner Martini POPC membrane and WALP16 lowers the free energy of the transmembrane state, making it roughly equal to that of the interfacial state. This change goes into the right direction, but it does not eliminate the pronounced minimum of the interfacial state, which is absent in the atomistic or PLUM data. This suggests that hydrophobic mismatch alone is not the sole reason for this feature.

To explore whether the strong hydrophobic mismatch of WALP16 in the 5-bead Martini POPC membrane also affects the peptide, we monitored the N- to C-terminal alpha carbon distance as a function of  $z$  for all force fields

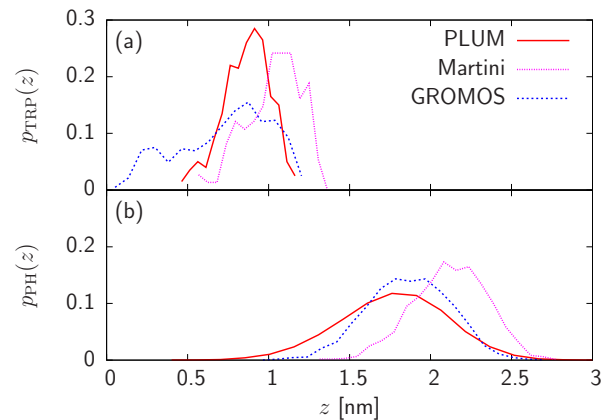


FIG. 3. Probability distributions of normal distances between the bilayer midplane and (a) the tryptophan side chains,  $p_{\text{TRP}}(z)$ , and (b) the lipid phosphate groups,  $p_{\text{PH}}(z)$ , for WALP16 in a POPC membrane modeled by PLUM, Martini, and GROMOS.

(Fig. 1 (d, e, f)) indicates a noticeable stretch for the Martini peptide in the region  $0 < z < 0.7$  nm, which coincides with the depth at which the peptide mostly samples a transmembrane helix (data not shown). WALP16 in POPC shows a gradual decrease of the N-C distance from 2.5 to 2.2 nm between  $z = 0$  and  $z \approx 2$  nm, while WALP16 in DMPC displays a sudden drop at  $z \approx 0.7$  nm, corresponding to the location of the free-energy barrier in Fig. 1 (b). Though Martini stabilizes a slightly *longer* helix around  $z = 0$ , compared to the other force fields, the apparent stretching indicates a strong driving force to better accommodate a short peptide in the bilayer. On the other hand, PLUM and the atomistic simulations (described in more details below) do not show any particular features close to the bilayer midplane. Unfortunately, the atomistic N-C-distance data show a lot of scatter, which is clearly a sampling issue.

For WALP16 in DMPC and WALP23 in POPC, the Martini model predicts a pronounced free energy barrier ( $\approx 4$  kcal/mol) for the transition from the interfacial to the transmembrane state. This is large enough to become a problem in unrestrained simulations that aim to study insertion: a peptide which enters the membrane from the aqueous phase could get trapped in the interfacial state without transitioning into the transmembrane state, even though the latter has a free energy that is lower by about 7 kcal/mol. Hall *et al.* have indeed encountered this difficulty during a study that aimed to quantify the insertion thermodynamics of various WALP peptides in different membranes (using an adapted version of Martini).<sup>50</sup> They resorted to co-assembling the lipid bilayer in the presence of a WALP peptide and doing statistics of the final state thus obtained (inserted or interfacially bound). This protocol suggests that simply beginning with an interfacially bound peptide was not an option, for it would rarely if ever proceed to fully

insert—a suspicion which the authors explicitly confirm.

Despite the rather vivid differences in the shape of the PMF, PLUM and Martini largely agree on the free energy of insertion into the transmembrane state (meaning,  $z = 0$ ), provided the hydrophobic mismatch is relaxed. This is not completely unexpected, for both models reproduce the PMFs of insertion of single amino-acid side-chains into a PC bilayer.<sup>27,41</sup> The finding is nevertheless nontrivial, because the absolute values do *not* agree with the atomistic ones, as we will discuss below.

Fig. 1 (c) shows the PMF of WALP16 in POPC, using the atomistic GROMOS force field.  $F(z)$  is largely downhill. It exhibits a small shoulder at  $z = 1$  nm, but no significant barrier. The location of this shoulder is close to the point at which the Martini model finally transitions from interfacial to transmembrane, suggesting that this might indeed be the physical origin of this feature, but the substantial increase in  $F(z)$  by about 10 kcal/mol between 1.7 nm and 0.7 nm (observed with Martini) is absent. Hence, the general shape of the PMF as predicted by the PLUM model appears closer to the atomistic data.

Finally, we wish to point out a curious discrepancy between both CG models and the atomistic reference: in both CG cases the free energy of WALP16 in its equilibrium state (about  $-20$  kcal/mol) is only 2/3 of the value predicted in the atomistic simulation (about  $-35$  kcal/mol). This is surprising, because both models capture the free energy of insertion of individual amino acids, as predicted atomistically. And while especially in the atomistic case one should always be wary of sampling issues,<sup>51</sup> and bootstrapping tends to underestimate error bars, we do not believe that this is the source of the discrepancy, for it would not suffice to explain a shift by 15 kcal/mol. Hence, it seems that the difference is real and has interesting consequences for modeling. Specifically, it should be clear that the free energy of insertion of an  $\alpha$ -helix consisting of  $N$  hydrophobic amino acids is not simply the sum of the free energy of insertion of each individual amino acid, because there are correlation and cooperativity effects. It seems likely that these effects depend not just on the physics captured on the coarse-grained level but on more local effects, too. If so, CG models of peptides will not capture the insertion free energy correctly, even if ostensibly parametrized for precisely that, and the difference might even be model dependent. Given the large amount of research undertaken with these models, it would appear crucial to understand this issue better.

## B. Folding in the membrane

Since the PLUM force field was designed to model changes in secondary structure, we can probe the free-energy landscape of WALP as a function of helicity—using appropriate techniques to ensure accurate sampling. Hamiltonian replica exchange molecular dynamics (HREMD) simulations inside the membrane combined

with the weighted histogram analysis method (WHAM; Appendix D) yields the free energy profiles shown in Fig. 4. Unsurprisingly, the helical state corresponds to the free-energy minimum.<sup>21</sup> We note a slight increase in the free energy when the helicity approaches 1, illustrative of some fraying at the ends of the chain. The low-helicity states, on the other hand, are highly suppressed, with free-energy differences ranging from 15 to 30 kcal/mol. Low but non-zero helicity ( $\approx 0.1$ ) is never observed due to the secondary-structure prediction algorithm, which relies on the presence of several ( $\approx 4$ ) consecutive amino acids with appropriate hydrogen-bonds and dihedrals to assign them in a helical state. We observe a plateau at low helicity (i.e., 0 – 0.3) followed by a sharp, apparently-downhill profile to the helical state. Overall, we observe a strong chain-length dependence on the free-energy profile. If we plot the three curves against the number of broken backbone hydrogen bonds (data not shown), the three curves agree more closely in the vicinity of their minima, because the change in helicity per broken hydrogen bond depends on the peptide’s length.

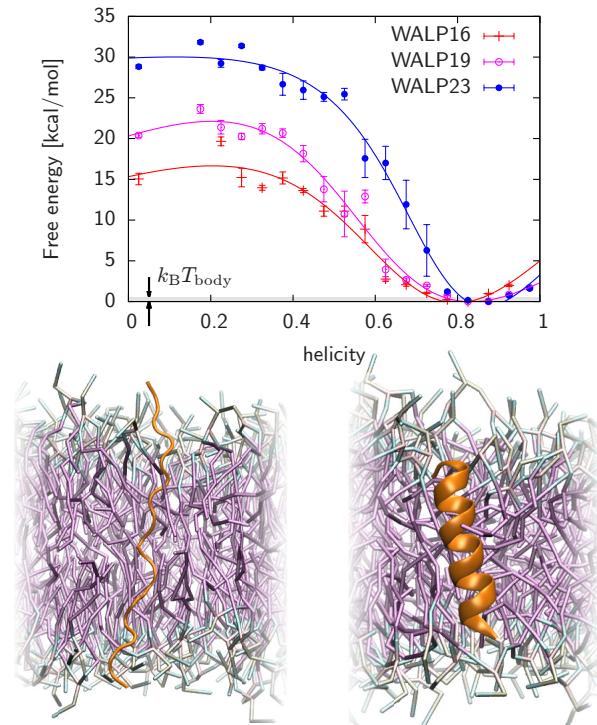


FIG. 4. Free energy as a function of helicity for WALP{16,19,23} inserted in the membrane using the CG PLUM force field. Solid lines are mere guides to the eye. The grey area roughly indicates the amount of thermal energy at body temperature. The conformations underneath illustrate an unstructured and helical conformations of WALP16 in the membrane. The PLUM energies are mapped from the reduced unit  $\mathcal{E} = 0.617$  kcal/mol.

### C. Folding in water

We then repeat the free energy study as a function of helicity from the previous section, but now for WALP dissolved in pure water. Fig. 5 (a) shows the free-energy profile of the WALP{16,19,23} peptides simulated using the CG PLUM force field. Just like in the membrane, we find a strong preference for helical conformations, with free-energy differences between coil and helix in the range  $\Delta F \approx 10 - 25$  kcal/mol.

Interestingly the chain length dependence of the free-energy is qualitatively different from the membrane case: while WALP16 again exhibits the lowest free energy at any value of the helicity, the profiles for WALP19 and WALP23 are remarkably similar. The qualitative difference between the two environments is noteworthy, since hydrogen bonds are the most likely contributors to the free-energy difference. The hydrophobicity will also play a larger role in an aqueous environment, as compared to the membrane. Yet the interaction strength of hydrogen bonds in the model does not depend on whether a bead is surrounded by water or lipids.<sup>27</sup> The only noticeable difference between the formation of a hydrogen bond in water and in the membrane results from the change between an implicit-water to an explicit-membrane environment, suggesting an entropic contribution of the model itself. Interestingly, we also observed a noticeable change in the stability of hydrogen bonds when transferring a helix from the water to the membrane environment.<sup>27</sup> Overall, this behavior may point at a complex interplay between the enthalpy (i.e., hydrogen-bonds) and entropy of helix formation in water,<sup>34</sup> while hydrophobic residues immersed in a hydrophobic environment provide more straightforward behavior.

The free-energy profiles shown in Figs. 4 and 5 (a) are consistent with the insertion process observed in Sec. III A: the system sampled a majority of helical conformations both in the fully transmembrane state and in the aqueous region where the peptide has left the membrane (Fig. 2 (a) and (e)).

We aimed at comparing these findings against reference atomistic simulations. Using metadynamics,<sup>52</sup> we computed the equivalent free-energy profile for WALP16 in water (Fig. 5 (b)). The profile shows a minimum at 80% helicity, which roughly corresponds to 10 over the 12 possible hydrogen bonds in the peptide, (indicative of light fraying of the helix). We observe a fairly complex profile with multiple minima, all located above the helical state. The helix is therefore the most favorable conformation according to these simulations. Compared to the CG results, we find a much narrower profile around the minimum. This discrepancy may partially be attributed to the difference in defining hydrogen bonds between the CG and atomistic simulations (see Appendices A and C). This also impacts the free energy at low helicity: while STRIDE’s definition of a hydrogen bond does not allow us to observe any low-helicity conformation (value around 0.1) in the CG profile, the observable in the metadynam-

ics is continuous along the entire range.

Aside from difficulties to compare the two curves, we point at a possible lack of sampling: the complexity of the system makes this free-energy profile difficult to accurately estimate using an atomistic model. The three curves shown in Fig. 5 (b), representing the profile after simulation times  $t = 125, 150,$  and  $180$  ns per replica, are illustrative of the convergence of the profile. We thus withhold from further interpreting this curve, and only conclude that the helix may indeed be a relevant conformation for WALP16 in solution.

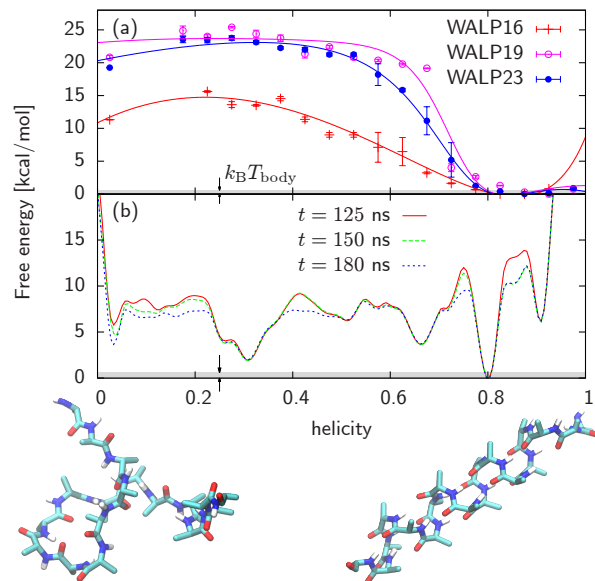


FIG. 5. Free energy as a function of helicity for WALP in water using (a) CG PLUM simulations on WALP{16,19,23} and (b) atomistic simulations on WALP16. Solid lines in (a) are mere guides to the eye. The three curves in (b) show the profile at different simulation times per replica, i.e.,  $t = 125, 150,$  and  $180$  ns. Note the different scales between (a) and (b). The grey area roughly indicates the amount of thermal energy at body temperature. The CG conformations underneath illustrate random coil and helical states of WALP16 in water. The PLUM energies are mapped from the reduced unit  $\mathcal{E} = 0.617$  kcal/mol.

## IV. CONCLUSIONS

We performed state-of-the-art thermodynamic calculations on WALP peptides interacting with a model phospholipid membrane using both coarse-grained (CG) and atomistic force fields. The potential of mean force (PMF) as a function of penetration depth  $z$  indicates increasing stability as WALP inserts into the membrane. PLUM and GROMOS yield qualitatively similar features: an almost-downhill process from water to the fully-inserted transmembrane state. Martini, on the other hand, predicts a distinct minimum for the interfacially bound

state, which goes along with a pronounced free-energy barrier for the transition from the interfacial to the transmembrane state for all cases we studied. For WALP16 in 5-bead POPC this interfacial minimum even becomes the global one, in contrast to both PLUM and GROMOS simulations. Similar behavior was reported in a previous Martini study of WALP16 as a function of different lipid-tail sizes, where the transmembrane WALP helix spontaneously flipped to the interfacial state in the presence of the longer lipids.<sup>48</sup> Though the role of negative hydrophobic mismatch seems to be predominant here, linking this behavior to particular aspects of the force field remains difficult.

Strikingly, PLUM and Martini report very similar free-energies of insertion at the bilayer midplane for WALP23 in POPC. The agreement likely results from the two models’ ability to reproduce the insertion of single amino acids in the bilayer, despite drastically different parametrization strategies.<sup>27,41</sup> On the other hand, the atomistic GROMOS simulations suggest increased stability of the transmembrane helix in the membrane: the atomistic WALP16 curve corresponds roughly to the insertion of WALP23 in the CG simulations, yielding a discrepancy of  $\approx 15$  kcal/mol. The fact that the two CG models underestimate the free energy of insertion by the same amount hints at missing correlation and cooperativity effects beyond the parametrization of individual amino acids. This poses questions concerning the coarse-graining strategies for peptides on which both PLUM and Martini rely, most importantly: under what conditions do matched thermodynamics on the amino acid level transfer up to the level of a full peptide? And if it does not, what are the dominant sources of discrepancy and can we correct for them?

Though Martini enforces secondary structure, making it unable to study the impact of the environment on folding, PLUM’s parametrization did allow us to probe this behavior in both water and the membrane. Folding in the membrane is strongly driven toward the helical state. We find roughly linear chain-length dependence on the free-energy profile, with longer peptides increasingly penalizing unstructured random coils.

Folding in water yielded similar behavior as in the membrane, though the chain-length dependence seems rather different, likely owing to the complex interplay between secondary structure—hydrogen bonds—and tertiary structure—hydrophobicity.<sup>34</sup> The results were compared with atomistic metadynamics simulations, which also indicate the helix as the most favorable conformation. Differences in the hydrogen-bond definition, as well as sampling difficulties of the atomistic model, make it hard to draw further conclusions. Nevertheless, both models suggest the helix as a reasonable conformation for WALP in water.

Overall, these findings suggest that enforcing the structure of a helix throughout the insertion process may reasonably describe the relevant conformational ensemble of states. In this sense, Martini’s lack of peptide structural

rearrangement does not strongly impinge on the results for WALP. A better understanding of the contribution of (un)folding during the insertion process will require the study of a different peptide that shows significantly different folds in water and the membrane. A systematic comparison of such biomolecular processes using very different computational models (e.g., atomistic vs. coarse-grained or flexible vs. rigid secondary structure) provides a better understanding of the impact of their underlying assumption to large-scale thermodynamic properties.

## ACKNOWLEDGMENTS

We appreciate constructive feedback by Siewert-Jan Marrink on several aspects of this work. We also thank Raffaello Potestio and Joseph F. Rudzinski for a critical reading of the manuscript. MD acknowledges partial support from NSF grant MCB-1330226. WFDB thanks the Sir Frederick Banting Fellowship Program of Natural Sciences and Engineering Research Council of Canada for financial support.

## Appendix A: PLUM simulation details

PLUM’s CG units were constructed from a length  $\mathcal{L} = 1 \text{ \AA}$ , an energy  $\mathcal{E} = k_B T_{\text{body}} \approx 0.617 \text{ kcal/mol}$  at  $T_{\text{body}} = 310 \text{ K}$ , and a mass  $\mathcal{M}$ . The time unit  $\tau = \mathcal{L}\sqrt{\mathcal{M}/\mathcal{E}} \sim 0.1 \text{ ps}$  does not properly reflect the dynamics of the system, due to the reduction of molecular friction during coarse-graining.<sup>28</sup>

We ran all simulations with the ESPRESSO molecular dynamics package.<sup>53</sup> A Langevin thermostat and modified Andersen barostat<sup>54</sup> produced an ensemble with constant temperature ( $T = 1.0 \mathcal{E}/k_B$ ), lateral tension ( $\Sigma = 0$ ), and vertical box height. Faster integration of the equations of motion was achieved using a multi-timestepping algorithm, setting the short and long time steps to  $\delta t = 0.01 \tau$  and  $\Delta t = 0.04 \tau$ , respectively.<sup>55</sup> A 288-POPC lipid membrane was used for all simulations. Each peptide was modeled without explicit termini. The helicity was determined from the STRIDE secondary-structure-prediction algorithm.<sup>56</sup> More simulation and system-setup details are described elsewhere.<sup>27,28</sup>

Hamiltonian replica exchange molecular dynamics (HREMD)<sup>57</sup> provided enhanced sampling of a peptide in both water and the membrane. In particular, we tuned the strength of the peptide’s hydrogen-bond interaction, i.e., the prefactor  $\epsilon$  of a modified Lennard-Jones potential with added directionality (see Appendix D).<sup>28</sup> The strength of the interaction was modulated by a prefactor,  $\lambda$ , where  $\lambda \geq 0$ . We ran HREMD simulations at prefactor values from  $\lambda = 0.1$  to  $\lambda = 1.0$ , spanning an appropriate range of conformational space from fully helical to the complete absence of any helical motif. We used 10 and 20 replicas for WALP{16,19} and WALP23, respectively. Each replica was run for at least  $10^6 \tau$ .



To probe insertion thermodynamics, the distance from the bilayer midplane to the peptide was measured from the  $z$ -coordinate (i.e., along the bilayer normal) of the center of mass of the lipid bilayer to the  $z$ -coordinate of the center of mass of the peptide. Umbrella sampling<sup>58</sup> restrained the sampled conformational space by restraining the normal distance between the  $z$ -coordinates of the membrane and the peptide. A harmonic restraint of spring constant  $k = 2 \mathcal{E}/\text{\AA}^2$  was applied at 1 \text{\AA} intervals, ensuring enough overlap between the different windows. In addition, difficulties associated with sampling PMFs of a solute in a lipid membrane<sup>51</sup> were addressed here by coupling the umbrella sampling with HREMD. Each umbrella restraint was simulated at 4 interaction prefactors  $\lambda \in \{0.55, 0.70, 0.85, 1.00\}$  to help sample the conformational flexibility of the peptide. Each replica was run for  $10^5 \tau$ , providing an aggregate time of  $2 \times 10^7 \tau$  for each peptide.

All enhanced-sampling methodologies were unbiased using the weighted histogram analysis method (WHAM; see also Appendix D).<sup>59–61</sup> All error bars were calculated from bootstrapping.<sup>62</sup>

### Appendix B: Martini simulation details

GROMACS v4.6<sup>63</sup> was used for the Martini simulations. Martini 2.1<sup>29</sup> and 2.2P<sup>40,64</sup> models were used for the standard and polarizable water, respectively. A 10-fs time step was used, updating the neighbor list every 10 steps. Lennard-Jones interactions were shifted to zero between 0.9 and 1.2 nm. Electrostatic interactions were truncated after 1.2 nm with a shifted potential from 0 to 1.2 nm and a dielectric of 15 (2.5 for polarizable water). Although not recommended to be used in classical simulations, truncation can be used for Martini due to how the model has been parametrized.<sup>65</sup> The temperature of 310 K was maintained using the V-rescale thermostat<sup>66</sup> with a 1-ps time constant. Weak semi-isotropic pressure coupling was used with the Berendsen barostat (1-ps time constant and  $3 \times 10^{-4} \text{ bar}^{-1}$  compressibility)<sup>67</sup>. Small bilayer patches were simulated with 100 POPC lipids per leaflet (121 for the DMPC bilayer). We did not make use of specific termini groups.

We calculated the free energy for transferring a single WALP from water to the center of a POPC bilayer (and DMPC for Martini 2.2P). A cylindrical position restraint was applied from the  $C_\alpha$  of the center residue of WALP and the center of mass of lipids inside a 1.2-nm-radius cylinder centered around the peptide, applied along the direction normal to the plane of the bilayer. To prevent jumps at the cylinder’s interface, between 1.2 and 1.7 nm the weights are switched to zero. A force constant of 500 kJ/mol/nm<sup>2</sup> for the harmonic restraint was used and a 0.1-nm spacing between adjacent umbrella sampling simulations, from water (5 nm) to the bilayer center (0 nm). Each simulation was run for at least 500 ns. Free energy profiles were generated using the weighted histogram

analysis method (WHAM)<sup>60</sup> implemented in G\_WHAM<sup>68</sup>. Error bars were estimated using the bootstrap method<sup>62</sup> with 100 bootstraps.

### Appendix C: Atomistic simulation details

The final WALP16 structure from the Martini umbrella sampling simulations was converted back to atomistic representation using the BACKWARDS<sup>69</sup> method. The GROMOS 54a7 force field<sup>70</sup> was used on WALP, GROMOS on the POPC lipids,<sup>71</sup> and SPC<sup>72</sup> for water. We used a 2-fs time step with bonds to hydrogens constrained with the LINCS method.<sup>73</sup> The particle mesh Ewald summation method was used for long-range electrostatic interactions.<sup>65,74</sup> Lennard-Jones interactions were shifted from 0.9 to 1.0 nm and truncated there after. The V-rescale method<sup>66</sup> was used for temperature coupling with a reference temperature of 310 K and a 0.1 ps time constant. Pressure was maintained semi-isotropically at 1 bar using the Berendsen barostat,<sup>67</sup> a 2.5-ps time constant and  $4.5 \times 10^{-5} \text{ bar}^{-1}$  compressibility. For the umbrella sampling, we increased the harmonic force constant to 3000 kJ/mol/nm<sup>2</sup> and ran each simulation for 250 ns.

To compute the free energy of folding in water for WALP16, a combination of the metadynamics method and the parallel tempering scheme was used.<sup>52,75</sup> Ten replicas were simulated spanning a temperature range of 290 – 400 K. An exchange success probability of 9% was achieved by applying the well-tempered ensemble (WTE) approach, which evenly increases the spread of the potential energy distribution across replicas, while preserving the same ensemble averages.<sup>76,77</sup> The PTMetaD-WTE calculations were performed and analyzed with the PLUMED2 plugin.<sup>78</sup>

The PTMetaD-WTE simulations were performed for a total period of 180 ns/replica. The relative free-energy differences between all of the stable minima were monitored starting after 100 ns/replica and were unchanged after this point, so the simulation was terminated after an additional 80 ns/replica. The collective variables,  $s$ , biased in the simulations were a pairwise coordination number comprising all of the alpha-helical hydrogen bonds ( $i, i + 4$  pairs) and the peptide’s radius of gyration (alpha carbons only; for a discussion on selecting the collective variables and a comparison of the different metadynamics techniques, see Ref.<sup>79</sup>). The hydrogen-bond collective variable is formulated in PLUMED as a summation of switching functions of the form:

$$s = \sum_{i=1}^{12} \frac{1 - \left(\frac{r_{i,i+4}}{r_0}\right)^n}{1 - \left(\frac{r_{i,i+4}}{r_0}\right)^m} \quad (\text{C1})$$

with  $r_0 = 0.25$  nm,  $n = 6$ , and  $m = 9$  (note there are 12 possible  $\alpha$ -helical contacts in WALP16). These numbers were scaled by 12 to provide an approximate “fraction

of helicity” in the results. The metadynamics parameters were 0.2 and 0.01 nm for the Gaussian widths of the helicity and radius of gyration. Gaussians were deposited with a frequency of one per 2 ps, and the convergence of the free-energy estimate was controlled by using well-tempered metadynamics<sup>80</sup> and a bias factor of 10. As in previous work, an initial simulation period (10 ns/replica) was used to equilibrate the replicas to a variety of unfolded structures and build up the WTE energy bias to achieve overlap between the 10 replicas. This simulation used a bias factor of 40 and a Gaussian width of 450 kJ/mol. The results presented show a 1D projection of the 2D metadynamics free-energy surface.

#### Appendix D: Estimating free energies from HREMD using WHAM

The weighted histogram analysis method (WHAM) provides a minimum variance estimator of the density of states by combining several simulations of the same system.<sup>59,60</sup> The method is most useful when applied to a set of simulations that explore different parts of phase space, each contributing to the estimation of thermodynamic properties of the system. The sampling of phase space is enhanced by an appropriate choice of Hamiltonians or control parameters (e.g., temperature), which together help provide a representative sampling of phase space for the process of interest. Though originally applied to simulations at different temperatures,<sup>59</sup> in the following we vary the Hamiltonian of the original system,  $\mathcal{H} = \mathcal{H}_0 + V$ , where  $V$  corresponds to a specific part of the Hamiltonian, e.g., an interaction potential.

In this work, we vary the strength of the protein hydrogen-bond interaction potential<sup>28,31</sup>

$$V(r, \vartheta_N, \vartheta_C) = \epsilon_{\text{hb}} \left[ 5 \left( \frac{\sigma_{\text{hb}}}{r} \right)^{12} - 6 \left( \frac{\sigma_{\text{hb}}}{r} \right)^{10} \right] \quad (\text{D1})$$

$$\times \begin{cases} \cos^2 \vartheta_N \cos^2 \vartheta_C, & |\vartheta_N|, |\vartheta_C| < 90^\circ \\ 0 & \text{otherwise} \end{cases}$$

Each simulation  $k$  corresponds to the Hamiltonian  $\mathcal{H}_k = \mathcal{H}_0 + \lambda V$ , where  $\lambda > 0$ .  $\lambda = 1$  thus corresponds to the original Hamiltonian,  $\mathcal{H}$ , while  $\lambda \neq 1$  alters the propensity to form hydrogen bonds.

Assuming that all simulations were run at the same inverse temperature  $\beta = (k_B T)^{-1}$ , the calculation of the free energy as a function of parameter  $Q$  is provided by

$$\beta F(Q) \propto -\ln \left[ \sum_{i,s} \frac{\delta(Q - Q_{i,s})}{\sum_j N_j \exp[\beta(\lambda_i - \lambda_j)V_s - f_j]} \right], \quad (\text{D2})$$

where  $\delta(*)$  bins parameter  $Q$  in a discrete set,  $N_j$  is the number of samples of simulation  $j$ ,  $f_j$  is the scaled free energy of simulation  $j$ ,  $i$  and  $j$  sum over simulations, and  $s$  sums over samples.<sup>81</sup> Determination of the set of  $f_j$  can be obtained by different means.<sup>60,61,82,83</sup>

#### Appendix E: Elastic energy of area-leaflet asymmetry upon insertion

Consider a bilayer patch that has an area  $A_0$  at zero tension. If we insert an object into the upper leaflet that occupies an area  $a$ , the resulting compressive stresses will drive an expansion of that leaflet, which in turn puts the lower leaflet under tension. In equilibrium, the bilayer expands to an area  $A > A_0$ , in which a net zero tension arises as a balance of compressive and tensile stresses in the upper and lower leaflet, respectively. The resulting elastic energy contributes to the free energy of insertion of the object. How large is it?

If  $K_{A,m} = K_A/2$  is the monolayer stretching modulus, the total elastic energy can be written as

$$E_{\text{el}} = \frac{1}{2} K_{A,m} \frac{(A - A_0 - a)^2}{A_0} + \frac{1}{2} K_{A,m} \frac{(A - A_0)^2}{A_0}. \quad (\text{E1})$$

The still vanishing stress is given by

$$0 = \frac{\partial E_{\text{el}}}{\partial A} = K_{A,m} \left[ \frac{A - A_0 - a}{A_0} + \frac{A - A_0}{A_0} \right], \quad (\text{E2})$$

from which we find  $A = A_0 + a/2$ , showing that the area mismatch is shared evenly between the two leaflets. The total elastic energy is therefore

$$E_{\text{el}} = \frac{1}{8} K_A A_0 \left( \frac{a}{A_0} \right)^2. \quad (\text{E3})$$

For WALP, we estimate the area of the inserted object as  $a = \pi(d/2)^2$ , where  $d = 12 \text{ \AA}$  is the diameter of an  $\alpha$ -helix. In our simulations, we use a relaxed membrane area  $A_0 = (100 \text{ \AA})^2$ , such that  $(a/A_0)^2 \sim 10^{-4}$ . Given a typical value  $K_A \approx 250 \text{ mN/m}$  for the stretching modulus,<sup>84</sup> we obtain  $E_{\text{el}} \sim 0.1 k_B T \sim 0.06 \text{ kcal/mol}$ , which is a negligible contribution to the overall free energy of insertion.

- <sup>1</sup>J. Israelachvili, S. Marčelja, and R. G. Horn, Quarterly reviews of biophysics **13**, 121 (1980).
- <sup>2</sup>D. Eisenberg, Annual review of biochemistry **53**, 595 (1984).
- <sup>3</sup>J. E. Darnell, H. F. Lodish, D. Baltimore, *et al.*, *Molecular cell biology*, Vol. 2 (Scientific American Books New York, 1990).
- <sup>4</sup>M. Edidin, Nature Reviews Molecular Cell Biology **4**, 414 (2003).
- <sup>5</sup>G. von Heijne, Annual review of biochemistry **80**, 157 (2011).
- <sup>6</sup>X. Li, P. Mooney, S. Zheng, C. R. Booth, M. B. Braunfeld, S. Gubbens, D. A. Agard, and Y. Cheng, Nature methods **10**, 584 (2013).
- <sup>7</sup>S. Boutet, L. Lomb, G. J. Williams, T. R. Barends, A. Aquila, R. B. Doak, U. Weierstall, D. P. DePonte, J. Steinbrener, R. L. Shoeman, *et al.*, Science **337**, 362 (2012).
- <sup>8</sup>G. R. Bowman, V. A. Voelz, and V. S. Pande, Current opinion in structural biology **21**, 4 (2011).
- <sup>9</sup>K. A. Dill and J. L. MacCallum, Science **338**, 1042 (2012).
- <sup>10</sup>E. A. Cino, W.-Y. Choy, and M. Karttunen, J Chem Theory Comput **8**, 2725 (2012).
- <sup>11</sup>S. Piana, J. L. Klepeis, and D. E. Shaw, Current opinion in structural biology **24**, 98 (2014).
- <sup>12</sup>E. Lindahl and M. S. Sansom, Current opinion in structural biology **18**, 425 (2008).

- <sup>13</sup>P. J. Booth and A. R. Curran, Current opinion in structural biology **9**, 115 (1999).
- <sup>14</sup>J. U. Bowie, Nature **438**, 581 (2005).
- <sup>15</sup>J.-L. Popot and D. M. Engelman, Biochemistry **29**, 4031 (1990).
- <sup>16</sup>J. U. Bowie, Current opinion in structural biology **21**, 42 (2011).
- <sup>17</sup>J. A. Killian, I. Salemk, M. R. de Planque, G. Lindblom, R. E. Koeppe, and D. V. Greathouse, Biochemistry **35**, 1037 (1996).
- <sup>18</sup>S. Morein, E. Strandberg, J. A. Killian, S. Persson, G. Arvidson, R. Koeppe 2nd, and G. Lindblom, Biophysical journal **73**, 3078 (1997).
- <sup>19</sup>E. Strandberg, S. Özdirekcan, D. T. Rijkers, P. C. van der Wel, R. E. Koeppe, R. M. Liskamp, and J. A. Killian, Biophysical journal **86**, 3709 (2004).
- <sup>20</sup>W. Im and C. L. Brooks, Proceedings of the National Academy of Sciences of the United States of America **102**, 6771 (2005).
- <sup>21</sup>S. K. Kandasamy and R. G. Larson, Biophysical journal **90**, 2326 (2006).
- <sup>22</sup>S. Özdirekcan, C. Etchebest, J. A. Killian, and P. F. Fuchs, Journal of the American Chemical Society **129**, 15174 (2007).
- <sup>23</sup>L. Monticelli, D. P. Tieleman, and P. F. Fuchs, Biophysical journal **99**, 1455 (2010).
- <sup>24</sup>T. Kim and W. Im, Biophysical journal **99**, 175 (2010).
- <sup>25</sup>H. Nymeyer, T. B. Woolf, and A. E. Garcia, Proteins: Struct., Funct., Bioinf. **59**, 783 (2005).
- <sup>26</sup>M. B. Ulmschneider, J. P. Doux, J. A. Killian, J. C. Smith, and J. P. Ulmschneider, Journal of the American Chemical Society **132**, 3452 (2010).
- <sup>27</sup>T. Bereau, Z.-J. Wang, and M. Deserno, J. Chem. Phys. **140**, 115101 (2014).
- <sup>28</sup>T. Bereau and M. Deserno, The Journal of membrane biology **248**, 395 (2014).
- <sup>29</sup>S. J. Marrink, H. J. Risselada, S. Yefimov, D. P. Tieleman, and A. H. De Vries, The Journal of Physical Chemistry B **111**, 7812 (2007).
- <sup>30</sup>P. J. Bond, C. L. Wee, and M. S. Sansom, Biochemistry **47**, 11321 (2008).
- <sup>31</sup>T. Bereau and M. Deserno, J. Chem. Phys. **130**, 235106 (2009).
- <sup>32</sup>Z.-J. Wang and M. Deserno, J. Phys. Chem. B **114**, 11207 (2010).
- <sup>33</sup>Z.-J. Wang and M. Deserno, New J. Physics **12**, 095004 (2010).
- <sup>34</sup>T. Bereau, M. Bachmann, and M. Deserno, J. Am. Chem. Soc. **132**, 13129 (2010).
- <sup>35</sup>T. Bereau, M. Deserno, and M. Bachmann, Biophys. J. **100**, 2764 (2011).
- <sup>36</sup>K. L. Osborne, M. Bachmann, and B. Strodel, Proteins: Structure, Function, and Bioinformatics **81**, 1141 (2013).
- <sup>37</sup>T. Bereau, C. Globisch, M. Deserno, and C. Peter, J. Chem. Theory Comput. **8**, 3750 (2012).
- <sup>38</sup>D. Reith, M. Pütz, and F. Müller-Plathe, Journal of computational chemistry **24**, 1624 (2003).
- <sup>39</sup>J. L. MacCallum, W. Bennett, and D. P. Tieleman, Biophys. J. **94**, 3393 (2008).
- <sup>40</sup>D. H. de Jong, G. Singh, W. D. Bennett, C. Arnarez, T. A. Wassenaar, L. V. Schäfer, X. Periole, D. P. Tieleman, and S. J. Marrink, Journal of Chemical Theory and Computation **9**, 687 (2012).
- <sup>41</sup>L. Monticelli, S. K. Kandasamy, X. Periole, R. G. Larson, D. P. Tieleman, and S.-J. Marrink, Journal of chemical theory and computation **4**, 819 (2008).
- <sup>42</sup>C. A. López, A. J. Rzepiela, A. H. De Vries, L. Dijkhuizen, P. H. Hunenberger, and S. J. Marrink, Journal of Chemical Theory and Computation **5**, 3195 (2009).
- <sup>43</sup>T. Bereau and K. Kremer, Journal of Chemical Theory and Computation (2015).
- <sup>44</sup>H. I. Ingólfsson, M. N. Melo, F. J. van Eerden, C. Arnarez, C. A. Lopez, T. A. Wassenaar, X. Periole, A. H. De Vries, D. P. Tieleman, and S. J. Marrink, Journal of the American Chemical Society **136**, 14554 (2014).
- <sup>45</sup>T. A. Wassenaar, H. I. Ingólfsson, R. A. Bockmann, D. P. Tieleman, and S. J. Marrink, Journal of Chemical Theory and Computation **11**, 2144 (2015).
- <sup>46</sup>D. I. Kopelevich, The Journal of chemical physics **139**, 134906 (2013).
- <sup>47</sup>W. Humphrey, A. Dalke, and K. Schulten, J. Mol. Graphics **14**, 33 (1996).
- <sup>48</sup>S. Ramadurai, A. Holt, L. V. Schäfer, V. V. Krasnikov, D. T. Rijkers, S. J. Marrink, J. A. Killian, and B. Poolman, Biophysical journal **99**, 1447 (2010).
- <sup>49</sup>W. L. Jorgensen, D. S. Maxwell, and J. Tirado-Rives, Journal of the American Chemical Society **118**, 11225 (1996).
- <sup>50</sup>B. A. Hall, A. P. Chetwynd, and M. S. Sansom, Biophysical journal **100**, 1940 (2011).
- <sup>51</sup>C. Neale, W. D. Bennett, D. P. Tieleman, and R. Pomès, J. Chem. Theory Comput. **7**, 4175 (2011).
- <sup>52</sup>A. Laio and M. Parrinello, Proceedings of the National Academy of Sciences **99**, 12562 (2002).
- <sup>53</sup>H.-J. Limbach, A. Arnold, B. A. Mann, and C. Holm, Comput. Phys. Comm. **174**, 704 (2006).
- <sup>54</sup>A. Kolb and B. Dünweg, J. Chem. Phys. **111**, 4453 (1999).
- <sup>55</sup>T. Bereau, Physics Procedia **68**, 7 (2015), DOI: 10.1016/j.phpro.2015.07.101.
- <sup>56</sup>D. Frishman and P. Argos, Proteins: Struct. Func. Genet. **23**, 566 (1995).
- <sup>57</sup>A. Bunker and B. Dünweg, Phys. Rev. E **63**, 016701 (2000).
- <sup>58</sup>G. M. Torrie and J. P. Valleau, J. Comput. Phys. **23**, 187 (1977).
- <sup>59</sup>A. M. Ferrenberg and R. H. Swendsen, Phys. Rev. Lett. **63**, 1195 (1989).
- <sup>60</sup>S. Kumar, J. M. Rosenberg, D. Bouzida, R. H. Swendsen, and P. A. Kollman, J. Comput. Chem. **13**, 1011 (1992).
- <sup>61</sup>T. Bereau and R. H. Swendsen, J. Comput. Phys. **228**, 6119 (2009).
- <sup>62</sup>M. R. Chernick, *Bootstrap Methods: A Guide for Practitioners and Researchers*, 2nd ed. (Wiley-Interscience, 2008).
- <sup>63</sup>B. Hess, C. Kutzner, D. Van Der Spoel, and E. Lindahl, Journal of chemical theory and computation **4**, 435 (2008).
- <sup>64</sup>S. O. Yesylevskyy, L. V. Schäfer, D. Sengupta, and S. J. Marrink, PLoS Comput Biol **6**, e1000810 (2010).
- <sup>65</sup>G. A. Cisneros, M. Karttunen, P. Ren, and C. Sagui, Chem Rev **114**, 779814 (2014).
- <sup>66</sup>G. Bussi, D. Donadio, and M. Parrinello, The Journal of chemical physics **126**, 014101 (2007).
- <sup>67</sup>H. J. Berendsen, J. P. M. Postma, W. F. van Gunsteren, A. Dinola, and J. Haak, The Journal of chemical physics **81**, 3684 (1984).
- <sup>68</sup>J. S. Hub, B. L. De Groot, and D. Van Der Spoel, Journal of Chemical Theory and Computation **6**, 3713 (2010).
- <sup>69</sup>T. A. Wassenaar, K. Pluhackova, R. A. Bockmann, S. J. Marrink, and D. P. Tieleman, Journal of Chemical Theory and Computation **10**, 676 (2014).
- <sup>70</sup>N. Schmid, A. P. Eichenberger, A. Choutko, S. Riniker, M. Winger, A. E. Mark, and W. F. van Gunsteren, European biophysics journal **40**, 843 (2011).
- <sup>71</sup>D. Poger, W. F. Van Gunsteren, and A. E. Mark, Journal of computational chemistry **31**, 1117 (2010).
- <sup>72</sup>H. J. Berendsen, J. P. Postma, W. F. van Gunsteren, and J. Hermans, in *Intermolecular forces* (Springer, 1981) pp. 331–342.
- <sup>73</sup>B. Hess, H. Bekker, H. J. Berendsen, J. G. Fraaije, *et al.*, Journal of computational chemistry **18**, 1463 (1997).
- <sup>74</sup>U. Essmann, L. Perera, M. L. Berkowitz, T. Darden, H. Lee, and L. G. Pedersen, The Journal of chemical physics **103**, 8577 (1995).
- <sup>75</sup>G. Bussi, F. L. Gervasio, A. Laio, and M. Parrinello, Journal of the American Chemical Society **128**, 13435 (2006).
- <sup>76</sup>M. Bonomi and M. Parrinello, Physical review letters **104**, 190601 (2010).
- <sup>77</sup>M. Deighan, M. Bonomi, and J. Pfaendtner, Journal of Chemical Theory and Computation **8**, 2189 (2012).
- <sup>78</sup>G. A. Tribello, M. Bonomi, D. Branduardi, C. Camilloni, and G. Bussi, Computer Physics Communications **185**, 604 (2014).
- <sup>79</sup>T. N. Do, W.-Y. Choy, and M. Karttunen, Journal of Chemical Theory and Computation **10**, 5081 (2014).

- <sup>80</sup>A. Barducci, G. Bussi, and M. Parrinello, Physical review letters **100**, 020603 (2008).
- <sup>81</sup>T. Bereau, *Unconstrained Structure Formation in Coarse-Grained Protein Simulations*, Ph.D. thesis, Carnegie Mellon University (2011).
- <sup>82</sup>M. R. Shirts and J. D. Chodera, The Journal of chemical physics **129**, 124105 (2008).
- <sup>83</sup>F. Zhu and G. Hummer, Journal of computational chemistry **33**, 453 (2012).
- <sup>84</sup>W. Rawicz, K. Olbrich, T. McIntosh, D. Needham, and E. Evans, Biophysical journal **79**, 328 (2000).